Journal of Alloys and Compounds 504 (2010) 27–31

Contents lists available at ScienceDirect

Journal of Alloys and Compounds

journal homepage: www.elsevier.com/locate/jallcom

Energy levels and photoluminescence properties of nickel-doped bismuth ferrite

Dillip K. Mishra, Xiaoding Qi*

Department of Materials Science and Engineering, National Cheng Kung University, No. 1 University Road, Tainan City 70101, Taiwan

ARTICLE INFO

Article history:
Received 24 February 2010
Received in revised form 14 May 2010
Accepted 22 May 2010
Available online 2 June 2010

Keywords:
$BiFeO_3$
Spectroscopy
Sol–gel

ABSTRACT

Ni-doped $BiFeO_3$ (BFO) films have been prepared using sol–gel method. Photoluminescence and optical absorption measurements were carried out for the grown films and observed four emissions at 451 nm, 468 nm, 513 nm and 689 nm. The band gap of the Ni-doped BFO was calculated from the absorption data to be 2.75 eV. The spectroscopic data were analyzed in conjunction with the results of conductivity vs. temperature measurements, which showed three different kinds of activation energies related to the defect and dopant levels inside the band gap. The observed emissions were attributed to the transitions from the oxygen vacancy, Bi^{2+} and Ni^{3+} levels, as well as the intrinsic band-to-band transition.

1. Introduction

Multiferroic $BiFeO_3$ (BFO) films have been deposited on a number of substrates. Although pulsed laser deposition (PLD) and RF magnetron sputtering have been used considerably for high phase-purity and accurate stoichiometry, there are wide varieties of methods available to grow BFO for optical studies. Irrespective of the growth methods such as microwave [1], hydrothermal and sol–gel [2,3], the optical gap of the samples with various microstructures were observed to be around 2.2 eV, which was far less than the theoretically calculated value of 2.8 eV [4]. Template synthesis of BFO nanowires produced an optical gap of 2.5 eV [5]. However, when BFO was obtained as a thin film using more controlled environments like PLD [6,7], molecule beam epitaxy [8], and sputtering [9], the optical gap was observed to be very close to the theoretical value. Nevertheless, sol–gel method of growing BFO films [10,11], which is a low temperature process with much less cost, can also produce pure phase having a wide range of optical gap, provided a decent route and suitable precursors are employed. Recent report by Choi et al. on the BFO photovoltaic properties has created a lot of attention in its optoelectronic applications [12]. Lately, the cathodoluminescence (CL) study of BFO films [9], as well as the photoluminescence (PL) study of BFO nanoparticles [13], added more interests within the scientific community for such kind of applications. However, for the photoelectronic devices, the conductivity of BFO is far too low, despite the leakage current problem that is often encountered in the studies of its ferroelectric properties [14,15]. Therefore, proper doping to increase the conductivity may be necessary. Doping of Ni^{2+} was reported to increase the BFO conductivity significantly [14]. Here, we are presenting the study of the optical properties of the Ni-doped BFO films grown by sol–gel method. In order to identify the defect energy levels relevant to the observed emissions, conductivity vs. temperature (σ–T) measurements were carried out to determine the activation energies. The band-gap structure was then drawn based on the information obtained from both the spectroscopic characterizations and σ–T measurements.

2. Experimental

The sol–gel was made out of bismuth nitrate and ferric nitrate according to the stoichiometric ratio and dissolved in the acetic acid and ethylene glycol monoethyl ether, respectively. Each precursor was dissolved in the respective solvent under constant stirring at a temperature of 45–50 °C for 30 min. After ensuring no sediments/precipitate, both precursors were mixed together and kept at 60 °C for 3–4 h. For doping purpose nickel acetate was used up to 5 at.%. The concentration of resultant solution was 0.2 M by adjusting the volume to 20 ml. Quartz and Pt coated Si were used as the substrates for the process. After the standard cleaning procedures using alcohol and DI water under sonication, the substrates were used for spin coating the gel. After each layer of coating at about 4000 rpm for 20 s, the film was kept at 60 °C for drying and then subsequent layers of coating were done. To obtain a desired thickness of the obtained film, we coated 10 layers of deposition on each substrate. The dried samples were heated up slowly in argon atmosphere until 300 °C, at which thermal gravity analysis showed that the gel had decomposed completely. The temperature was then quickly raised to a suitable final sintering temperature, which was tried at 500 °C, 550 °C and 600 °C, respectively, for 30 min. Earlier experiments on the sintering of room-temperature sputtered films found that such a short-time sintering in Ar was enough to form a well crystallized phase of BFO [16].

The thickness of the sintered films was measured by the α-step profilometer. The phase purity, composition, morphology, transparency and emission of the films were investigated by a range of techniques including X-ray diffraction (XRD), scanning electron microscopy (SEM), energy dispersive X-ray spectroscopy (EDS), X-ray photoemission spectroscopy (XPS), photoluminescence (PL) spectroscopy and UV–vis transmittance. The σ–T measurements were carried out in a vacuum chamber capable of heating the samples up to 800 °C.

* Corresponding author. Tel.: +886 6 2008060; fax: +886 6 2346290.
E-mail address: xqi045@mail.ncku.edu.tw (X. Qi).

0925-8388/$ – see front matter © 2010 Elsevier B.V. All rights reserved.
doi:10.1016/j.jallcom.2010.05.107

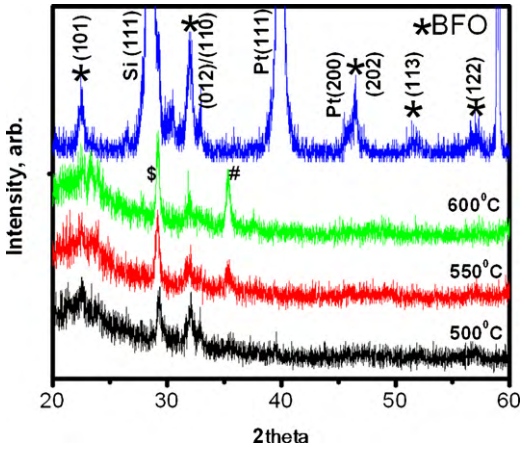

Fig. 1. XRD patterns of Ni-doped BFO films on quartz and Pt/Si substrates annealed at 500 °C, 550 °C and 600 °C. The reflection lines of BFO were indexed according to PDF 20-0169. #: Fe_2O_3 (PDF 73-0603), $: SiO_2 (PDF 75-1381).

3. Results and discussion

Fig. 1 shows the XRD of the sol–gel films on quartz substrate annealed at 500 °C, 550 °C and 600 °C. A film on Pt coated silicon substrate, which was heated at 500 °C for 30 min, is also shown for comparison. The BFO phase formation seems to be better when annealing was done at 500 °C, showing peaks at 22.5° and 32.16° which correspond to the (1 0 1) and (1 1 0) reflections. When the temperature of annealing was increased the peak at 32.16 becomes reduced and a new peak appears at 35.5°. This peak was due to the decomposition of dried gel to Fe_2O_3 (PDF 75-138) before the formation of BFO. The XRD results implied that BFO phase formation on quartz has been difficult as there are only two major peaks appeared in the spectrum, although nearly pure phase has been obtained from the temperature profile running through 250 °C till 500 °C. On using the same temperature profile for Pt coated silicon substrates, it was observed that the number of BFO peaks increased and has shown better crystallinity than the quartz ones (Fig. 1). The difficulty with the quartz substrates might result from the surface degradation of the substrates due to the crystallization of glass at high temperature. This speculation is supported by the XRD results (Fig. 1), which shows a characteristic diffraction peak of SiO_2 that becomes stronger and sharper as the sintering temperature increases. Fig. 2 belongs to the SEM micrographs of pure and Ni-doped BFO films. The films were composed of uniform BFO particles, but there was porosity as well as roughness. The average particle size was estimated using the SEM micrographs with a digital image analyzer, and it was found to be smaller for the doped films than the pure ones as can be seen from the plots of particle size distribution (Fig. 2c). The film thickness was observed to be 70 ± 15 nm by alpha step.

XPS analysis of BFO films shown in Table 1 indicates that the atomic ratio of Bi and Fe was 0.94 for the as grown samples, which was fairly close to the stoichiometric ratio of 1:1. But on treatment

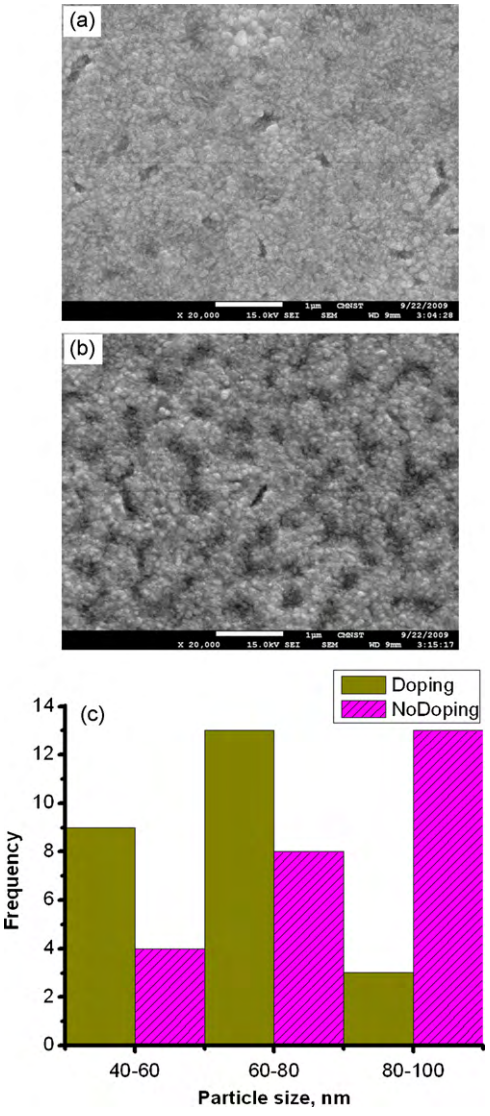

Fig. 2. Typical SEM micrographs of (a) pure and (b) Ni-doped sol–gel films prepared at 600 °C on quartz substrates. (c) Diameter distribution of BFO particles in the sol–gel films.

at 600 °C the ratio was increased to 3.97 or 3.39 for pure and Ni-doped films, respectively, indicating an excess of bismuth on the surface. However, on the EDS analyses of the same samples, a ratio of around 0.7 was indicated, showing a lack of bismuth instead. XPS is a true surface analysis, detecting the photoelectrons escaped from a few nanometer beneath the surface, while EDS has a typical penetration depth of 1 micrometer, which was able to see through the whole thickness of our films (~70 nm), So, it is understood that the disagreement between XPS and EDS came from the preferential evaporation of bismuth oxide due to its high vapor pressure, which

Table 1
Comparison of XPS and EDS data for the BFO films prepared at 600 °C.

Elements	XPS			EDS	
	As grown	After sintering at 600 °C		After sintering at 600 °C	
	No doping	No doping	Ni-doped	No doping	Ni-doped
Bi (at.%)	17.0	38.1	35.9	07.61	06.98
Fe (at.%)	18.1	09.6	10.6	10.86	10.01
O (at.%)	64.9	52.3	53.5	81.53	81.37
Ni (at.%)			<0.1		01.65

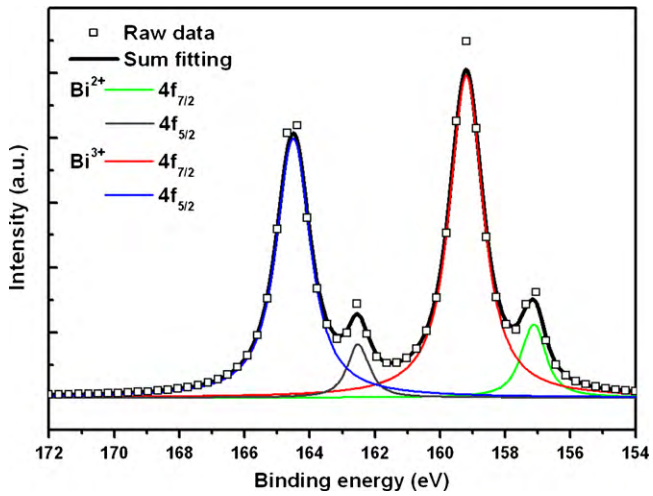

Fig. 3. The deconvolution of recorded XPS spectrum, showing the presence of Bi^{2+} in the BFO films.

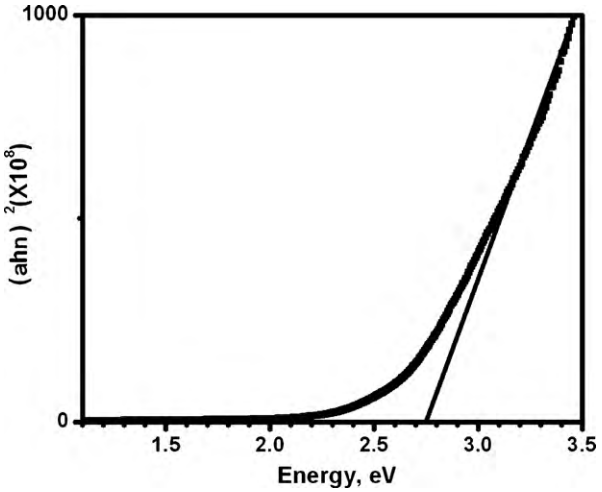

Fig. 5. Optical band gap of Ni-doped BFO film deposited on quartz at 500 °C.

caused an enrichment of bismuth on the film surface, while the overall content of the bismuth was deficient.

Preferential loss of bismuth at high temperature during thin film growth or bulk sintering of BFO has been widely speculated mainly based on the vapor pressure data. The above results provided convincing experimental evidence. Lower sintering temperature, e.g. 500 °C, produced BFO films of much more uniform composition, which also showed a better phase purity in XRD, as mentioned above. On the other hand, it is worth to mention that XPS observed a peak at 162.49 eV ($4f_{5/2}$), which was related to the lower-valence bismuth ions, in addition to the peak at 164.56 eV for the dominant trivalent Bi^{3+} [1,17], as shown in Fig. 3. The well-known leakage problem of BFO has often been attributed to the oxygen vacancies and/or mixed valence of iron [14,15,18]. This result indicates that mixed valence of bismuth may need to be taken into account as well.

Considering the potential optoelectronic applications of BFO in solar cells or photodetectors, etc., optical transmission studies were carried out for the sol–gel films grown on the quartz substrates. The optical properties of the films sintered at different temperatures gave more or less a similar transparency in visible and IR region, as shown in Fig. 4. The reduction of transparency at the short wavelength end for the sample prepared at 600 °C could be due to bismuth excess surface as evidenced from XPS data. The transparencies of more than 65% have been observed for all measured samples, which was comparable to the data of Xu and Shen [10]. From the transmittance/absorption spectra and the thickness of the films, the direct band gap of the film was calculated using the plot of $(\alpha h\nu)^2$ vs. photon energy. On extrapolating the linear part of the plot towards x-axis, the optical transition was observed to be at 2.75 eV as shown in Fig. 5. The transition at 2.75 eV was well matched with that of Xu and Shen [10] and other literature data [8].

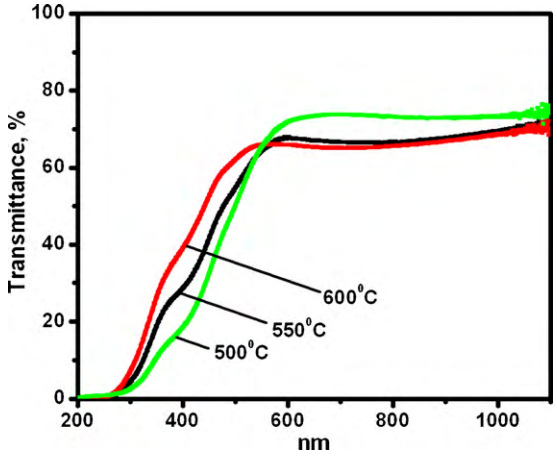

Fig. 4. Transmittance spectra of Ni-doped BFO films sintered at three different temperatures.

PL spectra of the sol–gel films gave out several broad weak emissions in the measured range from 425 to 750 nm as shown in Fig. 6. Although XRDs in Fig. 1 shows that different impurities were presented in the films sintered at 500 °C, 550 °C and 600 °C, the observed peak positions were the same (Fig. 6a), indicating that they came dominantly from the main phase, i.e. the BFO phase. The contributions of the impurities were reflected in the different backgrounds of the three samples. After deconvolution four peaks could be identified at 451 nm, 468 nm, 513 nm (Fig. 6a) and 689 nm (Fig. 6b). There were hardly any literatures available for the BFO emissions, until two recent reports by Yu and An [13] and Hauser et al. [9] which showed the emissions at about 454 nm and 515 nm for the Mn-doped BFO grown by wet chemical route at 400 °C, and the emissions at 454 nm, 506 nm and 563 nm for pure BFO films grown by RF sputtering at 550–650 °C. Table 2 presents the results of existing data and compared with the results obtained in this work.

Although we too observed a peak at 451 nm, deciphering all the observed peaks in the spectra was not straightforward. In principle, pure BFO only has the intrinsic emission arising from the band-to-band transitions. Any other emission of longer wavelengths must come from various defect and/or impurity (or dopant) levels inside the band gap. As just shown above, our Ni-doped BFO films had a slightly larger band gap, which was measured to be 2.75 eV, compared to 2.70 eV in the literature (Table 2). Therefore, the 451 nm peak, corresponding to the reported 454 nm in the literature, can be attributed unambiguously to the band-to-band transitions.

In order to identify the defect energy levels responsible for other emissions, σ–T curves were measured over a wide temperature range. Fig. 7 shows the Arrhenius plot of a typical σ–T curve for the 5 at% Ni-doped BFO, in which three kinds of slopes can be identified. At lower temperature (up to 225 °C) the activation of conduction was 0.12 eV, while at higher temperature (390–600 °C) it was 0.3 eV. When the temperature was intermediate (225–390 °C), the activation energy was observed to be 1.24 eV. First, the activation energy of 0.12 eV could be attributed to the lower-valence bismuth ions, which were observed in the XPS analyses of the samples. Bi^{2+}

Table 2
Comparison of optical characterization results for the BFO films.

Work	Process	Optical gap	Remark
Fruth et al. [11]	Wet chemistry film, 500 °C	2.59–2.82 eV	No PL study
Xu and Shen [10]	Sol–gel film, 550–650 °C	~2.70 eV	No PL study
Hauser et al. [9]	RF sputtered film, 500–600 °C	2.70 eV	3 CL peaks: 506 nm oxygen vacancy, 454 nm band edge emission, 563 nm suspected Bi vacancy
Yu and An [13]	Wet chemistry nanocrystals, 450 °C	No optical gap study	2 PL peaks: 454 nm self-activated center and 518 nm Mn^{2+} emission
This study	Sol–gel film, 500 °C, 550 °C, 600 °C	2.75 eV	4 PL peaks: 451 nm band-to-band emission, 468 nm emission from Bi^{2+}, 513 nm emission to Ni^{3+}, 689 nm emission from oxygen vacancy

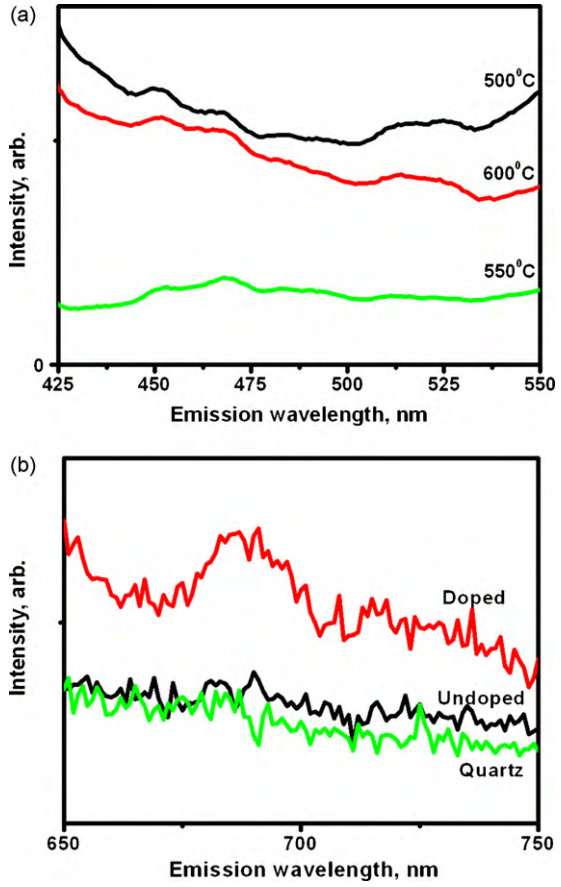

Fig. 6. (a) Room-temperature PL spectra of Ni-doped BFO films on the quartz substrate prepared at three different temperatures. (b) Comparison of the PL spectra for the pure and Ni-doped BFO films, as well as a blank quartz substrate.

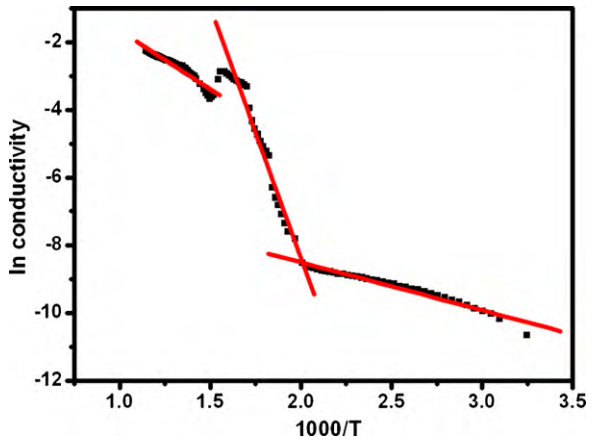

Fig. 7. Arrhenius plot of conductivity vs. temperature (σ–T) curve of 5% Ni-doped BFO.

could readily donate the extra $6p^1$ electron to the conduction band as a mobile carrier. The small activation energy was expected in view of the small difference between the oxidization energies of BiO and Bi_2O_3 [19]. The other two activation energies were most likely related to the nickel doping. The stable valence state of nickel was 2+. When Fe^{3+} in BFO was replaced by Ni^{2+}, charge compensation was required to keep overall charge neutrality. At low doping level, the charge compensation could be achieved by the creation of oxygen vacancies [14]. At increased doping level, more compensation mechanisms were required because a stable structure might only tolerate a limited amount of vacancies. Another feasible mechanism was to raise the valence of cations and the most likely cation to have the valence increased was Ni^{2+}, because the increase of ionization energy for $Ni^{2+} \rightarrow Ni^{3+}$ was only 70% of that for $Fe^{3+} \rightarrow Fe^{4+}$ [20].

Based on above discussion, the activation energy of 1.24 eV could be the energy required to release the electron trapped in oxygen vacancy, which is already well known to be a deep carrier-trap in many perovskites [21]. The measured value here was well within the range of 0.9–1.4 eV reported for typical oxygen vacancies [22]. Finally, the activation energy of 0.3 eV at higher temperature was due to Ni^{3+}. In contrast to Bi^{2+} and oxygen vacancy, Ni^{3+} is an acceptor ($Ni^{3+} + e^- \rightarrow Ni^{2+}$), whose energy level is indicated in the band structure in Fig. 8, along with those for Bi^{2+} and oxygen vacancy. The holes created by the thermal activation to this acceptor level were expected to have a low mobility due to the Coulomb attraction by the local negativity resulting from the substitution of Fe^{3+} by Ni^{2+}. Therefore, their contribution to the total conductivity was not observable in the σ–T curve until at higher temperature, after most of the trapped electrons in the oxygen vacancies were activated.

The observed emissions in the PL spectra can now be interpreted according to the band-gap structure, Fig. 8. 451 nm was the band-to-band transition as already discussed above. 468 nm was the transition from the Bi^{2+} level to the valence band. This level was 0.12 eV below the conduction band and therefore remained to be fairly populated at room temperature ($kT \sim 0.025$ eV), allowing the emission from this level to occur, which gave out the wavelength of 471 nm, as compared to the observed 468 nm in PL. The broad band transition centered at 513 nm was due to the capture

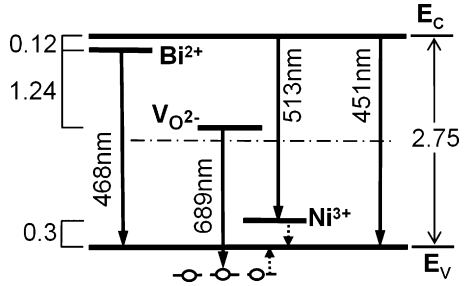

Fig. 8. Band-gap structure of BFO:5%Ni derived from the absorption, PL and σ–T measurements. The observed transitions are marked by the solid arrows.

of a mobile electron by the Ni^{3+}. As shown in Fig. 8, the energy difference between the bottom of conduction band and the Ni^{3+} level was 2.45 eV, corresponding to a wavelength of 506 nm, which was matched well with the PL result of 513 nm. Finally, the 689 nm peak might be attributed to the recombination of the electron trapped in oxygen vacancies with a deep hole in the valence band (VB), which was 0.3 eV below the top. The deep hole was created via a cross relaxation mechanism involving the Ni^{3+} level, as indicated by the dashed arrows in Fig. 8. The energy released from the relaxation of an electron at the Ni^{3+} level to the VB was used to excite an electron 0.3 eV below the top of VB up to the top, leaving behind a hole there. There is a similar process often observed in rare-earth or transition metal-doped crystals, which is called as cross relaxation and responsible for the concentration quenching [23]. As shown in Fig. 8, the transition between the oxygen vacancy level and the deep hole was 1.81 eV, corresponding to a wavelength of 685 nm, which was compared well to the PL data of 689 nm. In order to confirm this transition was indeed related to the nickel doping, the spectra of pure BFO and a blank quartz substrate were measured and compared with the doped one in Fig. 6b. It was only presented for the doped sample.

4. Conclusions

Ni-doped BFO films were grown using sol–gel method and their spectroscopic properties were studied in conjunction with the σ–T data, which showed three different kinds of activation energies related to the defect/dopant levels inside the band gap. The correlation of conductivity data with the photoluminescence properties was made for the first time here. Four luminescence peaks from samples produced in this work can be attributed to the transitions from the oxygen vacancy, Bi^{2+} and Ni^{3+} levels, as well as the intrinsic band-to-band transition,

Acknowledgements

This work was supported by the National Science Council under the grant number NSC-96-2628-E-006-010-MY3, and by the National Cheng Kung University (NCKU), Taiwan, via the Landmark Projects. Dr. Mishra would like to thank the Top University Project Office of the NCKU for providing a postdoctoral fellowship.

References

[1] U.A. Joshi, J.S. Jang, P.H. Borse, J.S. Lee, Appl. Phys. Lett. 92 (2008) 242106.
[2] S. Li, Y.H. Lin, B.P. Zhang, J.F. Li, C.W. Nan, J. Appl. Phys. 105 (2009) 54310.
[3] F. Gao, X.Y. Chen, K.B. Yin, S.A. Dong, Z.F. Ren, F. Yuan, T. Yu, Z.G. Zou, J.M. Liu, Adv. Mater. 19 (2007) 2889.
[4] S.J. Clark, J. Robertson, Appl. Phys. Lett. 90 (2007) 132903.
[5] F. Gao, Y. Yuan, K.F. Wang, X.Y. Chen, F. Chen, J.M. Liu, Z.F. Ren, Appl. Phys. Lett. 89 (2006) 102506.
[6] S.R. Basu, L.W. Martin, Y.H. Chu, M. Gajek, R. Ramesh, R.C. Rai, X. Xu, J.L. Musfeldt, Appl. Phys. Lett. 92 (2008) 91905.
[7] A. Kumar, R.C. Rai, N.J. Podraza, S. Denev, M. Ramirez, Y.H. Chu, L.W. Martin, J. Ihlefeld, T. Heeg, J. Schubert, D.G. Schlom, J. Orenstein, R. Ramesh, R.W. Collins, J.L. Musfeldt, V. Gopalan, Appl. Phys. Lett. 92 (2008) 121915.
[8] J.F. Ihlefeld, N.J. Podraza, Z.K. Liu, R.C. Rai, X. Xu, T. Heeg, Y.B. Chen, J. Li, R.W. Collins, J.L. Musfeldt, X.Q. Pan, J. Schubert, R. Ramesh, D.G. Schlom, Appl. Phys. Lett. 92 (2008) 142908.
[9] A.J. Hauser, J. Zhang, L. Mier, R.A. Ricciardo, P.M. Woodward, T.L. Gustafson, L.J. Brillson, F.Y. Yang, Appl. Phys. Lett. 92 (2008) 222901.
[10] Y. Xu, M.R. Shen, Mater. Lett. 62 (2008) 3600.
[11] V. Fruth, E. Tenea, M. Gartner, M. Anastasescu, D. Berger, R. Ramer, M. Zaharescu, J. Euro. Ceram. Soc. 27 (2007) 937.
[12] T. Choi, S. Lee, Y.J. Choi, V. Kiryukhin, S.W. Cheong, Science 324 (2009) 63.
[13] X.L. Yu, X.Q. An, Solid State Commun. 149 (2009) 711.
[14] X. Qi, J. Dho, R. Tomov, M.G. Blamire, J.L. MacManus-Driscoll, Appl. Phys. Lett. 86 (2005) 062903.
[15] Y.P. Wang, L. Zhou, M.F. Zhang, X.Y. Chen, J.M. Liu, Z.G. Liu, Appl. Phys. Lett. 84 (2004) 1731.
[16] X. Qi, W.C. Chang, J.C. Kuo, I.G. Chen, Y.C. Chen, C.H. Ko, J.C.A. Huang, J. Eur. Ceram. Soc. 30 (2010) 283.
[17] Y.H. Lee, J.M. Wu, Y.C. Chen, Y.H. Lu, H.N. Lin, Electrochem. Solid State Lett. 8 (2005) F43.
[18] V.R. Palkar, R. Pinto, Pramana J. Phys. 58 (2002) 1003.
[19] S.K. Sundaram, Bull. Mater. Sci. 14 (1991) 993.
[20] R.B. King (Ed.), Encyclopedia of Inorganic Chemistry, vol. 4, 2nd edition, John Wiley & Son Ltd., West Sussex, England, 2005, p. 2128.
[21] R. Waser, D.M. Smyth, in: C.P. De Araujo, J.F. Scott, G.W. Taylor (Eds.), Ferroelectric Thin Films: Synthesis and Basic Properties, Gordon and Breach Publishers, Amsterdam, 1996, p. 47.
[22] C. Kumar, R. Pascual, M. Sayer, J. Appl. Phys. 71 (1992) 865.
[23] J.G. Sole, L.E. Bausa, D. Jaque, An Introduction to the Optical Spectroscopy of Inorganic Solids, John Wiley & Sons Ltd., West Sussex, England, UK, 2005.